

# Progressive Sparse Local Attention for Video object detection

Chaoxu Guo<sup>1</sup>, Bin Fan<sup>1</sup>, Jie Gu<sup>1</sup>, Qian Zhang<sup>2</sup>,  
Shiming Xiang<sup>1</sup>, Veronique Prinet<sup>1</sup>, and Chunhong Pan<sup>1</sup>

<sup>1</sup>NLPR, CASIA

<sup>2</sup>Horizon Robotics

<sup>1</sup>{chaoxu.guo, bfan, jie.gu, prinet, smxiang, chpan}@nlpr.ia.ac.cn

<sup>2</sup>qian01.zhang@horizon.ai

## Abstract

Transferring image-based object detectors to domain of videos remains a challenging problem. Previous efforts mostly exploit optical flow to propagate features across frames, aiming to achieve a good trade-off between performance and computational complexity. However, introducing an extra model to estimate optical flow would significantly increase the overall model size. The gap between optical flow and high-level features can hinder it from establishing the spatial correspondence accurately. Instead of relying on optical flow, this paper proposes a novel module called Progressive Sparse Local Attention (PSLA), which establishes the spatial correspondence between features across frames in a local region with progressive sparse strides and uses the correspondence to propagate features. Based on PSLA, Recursive Feature Updating (RFU) and Dense feature Transforming (DFT) are introduced to model temporal appearance and enrich feature representation respectively. Finally, a novel framework for video object detection is proposed. Experiments on ImageNet VID are conducted. Our framework achieves a state-of-the-art speed-accuracy trade-off with significantly reduced model capacity.

## 1. Introduction

Object detection is a fundamental problem in computer vision and serves as a core technique in many practical applications, e.g. robotics, autonomous driving and human behavior analysis. With the development of convolutional neural networks (CNNs), remarkable successes have been achieved on detecting objects from images [7, 12, 13, 16, 17, 24, 26, 27, 29]. However, applying those techniques on a frame-by-frame basis to a video sequence is often unsatis-

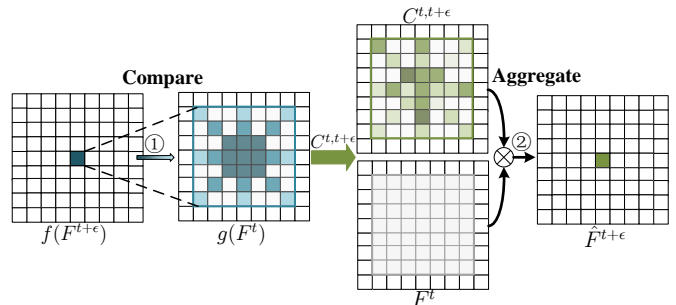


Figure 1. Illustration of Progressive Sparse Local Attention (PSLA). The goal of PSLA is to align feature map  $F_t$  with  $F^{t+\epsilon}$  in an attention way, which is formulated into two steps. The first step ① is that each feature cell in embedded feature map  $f(F^{t+\epsilon})$  compares to the surrounding cells in the embedded feature map  $g(F^t)$ , in a progressive sparser stride from center to outside. The resulting feature affinities are used to compute correspondence weights  $C^{t,t+\epsilon}$ , which capture the spatial correspondence between features. The second step ② is that the chosen feature cells in  $F^t$  are aggregated with the corresponding weights to generate a feature cell in  $\hat{F}^{t+\epsilon}$ , which is the aligned feature map from  $F^t$ .

factory due to the deteriorated appearance caused by motion blur, out-of-focus camera, and rare poses issues frequently encountered in videos. Conversely, the temporal information, absent from still images, provides rich cues which can be exploited during both training and testing.

Existing methods that leverage temporal information for object detection from videos mainly fall into two categories. The first one relies on dedicated post-processing [15, 19, 20, 22]. These methods firstly run image-based detector on single frames and then integrate the per-frame results by box-level post-processing. The last stage usually requires an extra object tracker or off-the-shelf optical flow to estimate motion field and associate the bounding boxes. Modeling temporal coherence in this way is sub-optimal

since detectors do not benefit from the temporal information when training.

Another category of methods [11, 32, 34, 36, 37, 38] exploits the temporal information in videos when training. They either pursue a trade-off between accuracy and computation cost or seek to improve performance at the expense of runtime. Among these methods, the optical flow is widely used to propagate the high-level features across frames. Extra optical flow models, e.g. FlowNet [9], have to be utilized to enable the end-to-end training and achieve a better performance. However, adding an optical flow model has drawbacks. First, extra model significantly increases the overall model size of detector (e.g., a typical detector of ResNet101+RFCN has 53M parameters and it has to add additional 37M parameters when using FlowNet.), which makes it harder to be deployed on mobile devices. Second, optical flow only establishes local pixel correspondences between two images. Directly transferring the flow field to high-level feature in the hierarchy may introduce artifacts. Because it ignores the transformation that happens from layer to layer in the network. Moreover, a shift of one pixel in high-level feature maps may correspond to up to ten to twenty pixels in the image, and it is very challenging for optical flow to capture such a large displacement.

Our work belongs to the second category. To address the limitations above, we propose a novel module, Progressive Sparse Local Attention (PSLA), which allows to propagate high-level semantic features across frames without relying on optical flow. Specifically, given two features  $F_t$  and  $F_{t+\epsilon}$  of frames  $I_t$  and  $I_{t+\epsilon}$  respectively, PSLA first produces correspondence weights based on the feature affinities between  $F_t$  and  $F_{t+\epsilon}$  and then aligns  $F_t$  with  $F_{t+\epsilon}$  by aggregating the feature with corresponding weights. It is similar to an attention mechanism [31] but different in that the attended positions in PSLA are distributed in a local region with progressive sparser stride as illustrated in Fig. 1, inspired by the motion distribution in videos as shown in 3.

In our framework for video object detection, expensive extraction of high-level features is performed on sparse key frames while low-cost extraction of low-level features is applied on dense non-key frames. Based on the extracted features, PSLA is used in two distinct and complementary situations: (1) to propagate high-level feature (at a given layer of the network) from a key frame to to a non-key frame. This allows to assign most of the computation cost to key frames and improves efficiency when testing without losing in accuracy. Moreover, a small network named *Quality Net* is devised to complement the propagated high-level feature with low-level information from features of non-key frames, in order to reduce the aliasing effect of feature propagation. We coin this procedure Dense Feature Transforming (DFT). (2) to maintain a temporal feature  $F_t$  and model temporal appearance of videos, by propagating high-level

features across key frames. Meanwhile, a *Update Net* is proposed to recursively update  $F_t$  with high-level features of key frames. We show experimentally that exploiting temporal context contributes to substantial gain in performance. We coin this procedure Recursive Feature Updating (RFU).

Extensive experiments are conducted on benchmark ImageNet VID [30] for video object detection. We demonstrate results that are on par with or outperform state-of-the-art methods in both speed and accuracy with reduced model capacity. In addition, we show that our model can generalise to the task of video object segmentation on the CityScapes dataset [6].

In summary, the contributions of this paper includes:

- We propose a novel module Progressive Sparse Local Attention (PSLA) to establish the spatial correspondence between feature maps without relying on extra optical flow models, which reduces model parameters significantly while achieves better results.
- Based on PSLA, two techniques, Recursive Feature Updating (RFU) and Dense Feature Transforming (DFT), are developed to model temporal appearance and enhance the feature representation of non-key frames, respectively.
- We introduce a novel framework for video object detection and it achieves a state-of-the-art speed accuracy trade-off on benchmark ImageNet VID [30].

## 2. Related Work

**Self-attention.** Self-attention is a mechanism first introduced in [31] for machine translation. To integrate enough context and long range information in a sequence, it computes the response at a position in a sequence by taking the weighted mean value of all positions, where the weights are learned by back propagation without explicit supervision. Bahdanau *et al.* [1] apply soft attention to machine translation aiming to capture soft alignments between source and target words. Unlike those previous works [1, 31], our proposed PSLA is a more general form of self-attention. In this paper it is applied in temporal spatial domain towards aligning two feature maps.

**Nonlocal and Local Operators.** Nonlocal is a traditional filter algorithm [2] that is widely used in image denoise [3, 23], super-resolution [14] and texture synthesis [10]. Those approaches compute response as a weighted mean of all the pixels in an image, where the weights are obtained based on the patch appearance similarity. More recently, based on the same principle, Wang *et al.* [33] develop a nonlocal operator utilized for video classification and object detection. It aims to capture long-range dependency within feature map and augments the receptive field.

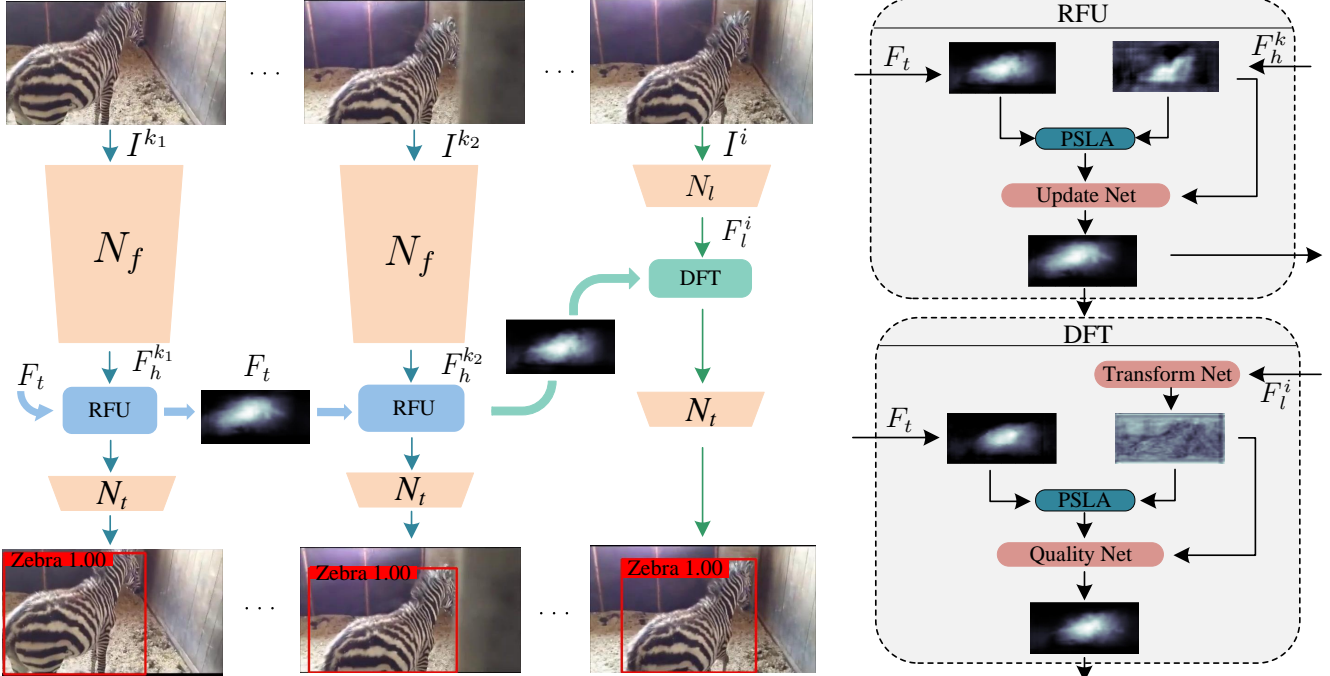


Figure 2. The pipeline of our framework. Only two key frames  $I^{k1}$ ,  $I^{k2}$  and one non-key frame  $I^i$  are shown for simplicity. Key frames are firstly fed into  $N_f$  to produce high-level features  $F_h^k$  while non-key frames are fed into a low-cost network  $N_l$  to extract low-level features  $F_l^i$ . Based on the high-level features, a temporal feature  $F_t$  is maintained to model temporal appearance of videos using *Recursive Feature Updating* (RFU), where  $F_t$  is updated recursively by *Update Net* with extracted high-level features  $F_h^k$  of new key frames. Meanwhile, *Densely Feature Transforming* (DFT) is utilized to propagated semantic features from updated  $F_t$  at nearest key frame, where *Quality Net* is employed to reduce aliasing effect of feature propagation from key frames to non-key frames. PSLA is embedded in RFU and DFT for feature alignment and propagation. The output of RFU or DFT is fed into  $N_t$  to produce the detection results.

At the other hand of the spectrum, Xiao *et al.* [34] propose a module to align features map in a local region. Our approach also aim at aligning feature maps, using a local operator. However, different from [34], we introduce sparsity in the local neighbourhood and use a *softmax* normalization to ensure that the most critical information is captured.

**Image Object Detection.** Existing state-of-the-art methods for image object detection mostly follow two paradigms, two-stage and single-stage. A two-stage pipeline consists of a generation of region proposals, region classification and location refinement. R-CNN [13] is a seminal work of two-stage methods. Fast R-CNN [12] improve the speed and accuracy by sharing computation of feature extraction while Faster R-CNN[29] learns to generate region proposals. Some following variants, *e.g.* R-FCN [7] and FPN [24], further improve the performance. Comparing to two-stage detectors, single-stage methods are more efficient but less accurate. Single Shot Detector (SSD)[26] produces detection results from default anchor boxes from multiple feature maps. YOLO [27, 28] instead formulate the detection as an regression problem. Lin *et al.* [25] propose focal loss to address the problem of data imbalance and develop a new detector named RetinaNet. In this paper we use R-FCN as our base detector.

**Video Object Detection.** Different from image object detection, methods for video detection should take temporal information into account. T-cnn [19] utilizes off-the-shelf optical flow to propagate bounding boxes. Then the boxes are re-scored and removed by considering temporal context of videos. Tpn [18] proposes a tubelet proposal network and employs a LSTM to incorporates temporal information from tubelet proposals. To boost the performance, MANet [32] and FGFA [37] use the optical flow estimated by FlowNet [9] to aggregate the feature of multiple nearby frames. Instead of relying on optical flow, D&T [11] predicts the bounding boxes of next frame by performing correlation between the features of current and next frame. To reduce the overall computation cost, Zhu *et al.* [38, 36] use the optical flow to propagate the high-level features of key-frames to other frames and avoids extracting expensive feature frequently. Chen *et al.* [4] improve both speed and accuracy by designing and optimizing a time-scale lattice. But an extra classifier is required to rescore the bounding boxes. It increases the model parameters greatly and can only be applied offline. The closest work to ours is STMN [34], which utilize a module similar to correlation to align feature maps in a local region. Conversely, our approach focus on a sparse neighborhood and softmax normalization is

utilized to better establish spatial correspondence. And our approach improve both speed and accuracy while STMN improves accuracy in expense of runtime.

### 3. Video Detection by Progressive Sparse Local Attention

#### 3.1. Overview of the Framework

The pipeline of our framework is illustrated in Fig. 2. Given a video, each frame is processed by a CNN to extract features, which is followed by a task network  $N_t$  for a specific task, such as object detection in this paper. On one hand, to save the computational cost, frames are divided into key frames and non-key frames, for which the feature extraction networks are different, denoted as  $N_f$  and  $N_l$  respectively. In order to limit the overall computation cost, the feature extraction network for non-key frames (i.e.,  $N_l$ ) should be a lightweight one since most of frames are non-key frames. On the other hand, to make use of the long term temporal information embedded in the video, a temporal feature  $F_t$  is maintained across the whole video, which is gradually updated at key frames by the proposed *Recursive Feature Updating* (RFU) module. Aided by the temporal feature, the semantic feature of a key frame will also be enhanced by RFU to benefit the final task. Meanwhile, due to the lightweight network used for non-key frames, their features are less powerful for the final task. For this reason, the *Densely Feature Transformation* (DFT) module is proposed to enrich their features by propagating from the temporal feature  $F_t$ . The key assumption for such a design is that the non-key frames are similar to nearby key frames so that their semantic features can be propagated from those of key frames. At the core of RFU and DFT is to align and propagate the temporal feature to that of the current processed frame (i.e.,  $F_h$  for a key frame and  $F_l$  for a non-key frame), which is addressed by the *Progressive Sparse Local Attention* (PSLA) method. In the following, we will describe in details of the proposed *Progressive Sparse Local Attention*, *Recursive Feature Updating* (RFU), and *Densely Feature Transformation*.

#### 3.2. Progressive Sparse Local Attention

The core of our framework is to align and propagate feature maps across frames. To this end, we introduce Progressive Sparse Local Attention (PSLA), a novel module that aims to establish spatial correspondence between two feature maps and propagate the feature maps with the correspondence.

PSLA proceeds by first computing correspondence weights based on the feature affinities between pairs of feature cells, originating from two distinct feature maps and distributed in progressive *sparser* strides (see Fig. 1). The motivation for this strategy is illustrated in Fig. 3: it shows

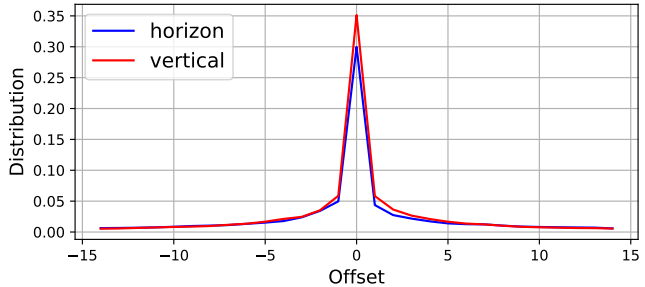


Figure 3. Optical flow field of sampled 100 ImageNet VID videos computed by FlowNet in horizon and vertical dimension. Best viewed in color.

that the marginal distribution of optical flow field along the vertical and horizon axis<sup>1</sup>, is largely concentrated around zero. This suggests that the feature cells used to compute correspondence weights can be limited to a close neighborhood with a progressive sparser stride. The progressive sparser stride enables PSLA to focus more on nearby positions, associated to small motions, and less on the positions far away, associated to larger motions.

Formally, let  $F^t$  and  $F^{t+\epsilon}$  be feature maps of frame  $I_t$  and  $I_{t+\epsilon}$  respectively, and their corresponding embedded features are denoted as  $f(F^t)$  and  $g(F^{t+\epsilon}) \in \mathbb{R}^{h \times w \times c}$ , where  $c$  is the number of channels of embedded feature maps. At this stage we aim to explain general operations of PSLA thus do not specify how  $F^t$  and  $F^{t+\epsilon}$  come from, which will be clarified in sections 3.3 and 3.4. The embedding functions  $f(\cdot)$  and  $g(\cdot)$  here are used to reduce the channel dimension of  $F^t$  and  $F^{t+\epsilon}$  for less computation cost. PSLA compares each feature cell from  $g(F^{t+\epsilon})$  to surrounding cells from  $f(F^t)$  at sparse locations in a local neighborhood. The resulting feature affinities are normalized to produce the weights used to align  $F^t$ , where feature cells with higher weights mean higher correspondence and account for higher proportion of the resulting feature cell. Finally the aligned features are propagated to frame  $I_{t+\epsilon}$ .

Specifically, the operation of PSLA can be formulated as two stages as follows.

The first stage is to produce sparse correspondence weights based on the feature affinities. Given two feature maps  $F^t$  and  $F^{t+\epsilon}$ , embedded via two functions  $f(\cdot)$  and  $g(\cdot)$ , the procedure of computing affinity between two feature cells is defined as

$$c_{ij} = \langle g(F_i^{t+\epsilon}), f(F_j^t) \rangle, \quad (1)$$

where  $i$  and  $j$  are position indices in each of the feature maps and  $g(F_i^{t+\epsilon}), f(F_j^t) \in \mathbb{R}^{1 \times 1 \times c}$ .  $\langle \cdot \rangle$  represents the inner product operation. For each location  $i$ , only the positions in  $\Phi(i)$  of  $f(F_j^t)$  are considered, which is a neighborhood with progressive sparser strides and a max displace-

<sup>1</sup>Precisely, optical flow field is computed with FlowNet[9], on 100 videos randomly sampled from ImageNet VID training split[30]

ment  $d$ . For clarity, we divide  $\Phi(i)$  into a series of sub-regions as

$$\Phi(i) = \{\Phi_1(i), \Phi_2(k), \dots, \Phi_d(i)\}, \quad (2)$$

where

$$\begin{aligned} \Phi_1(i) &= \Delta_1(i), \\ \Phi_k(i) &= \Delta_k(i) \setminus i, k > 1 \\ \Delta_k(i) &= [-k : k : k] \times [-k : k : k] + i, 1 \leq k \leq d, \end{aligned} \quad (3)$$

$\Delta_k(i)$  stands for the positions set in sub-region  $k$ , which ranges from  $-k$  to  $+k$  in a stride of  $k$  along both horizon and vertical axis, centered at  $i$ . The spatial arrangement of  $\Phi(i)$  in  $g(F^t)$  is shown in Fig. 1. It is designed as a progressive sparser grid. Regions of different color correspond to different sub-regions  $\Phi_k(i)$ . We can further compute the normalized correspondence weights:

$$\hat{c}_{ij} = \frac{\exp(c_{ij})}{\sum_{j \in \Phi(i)} \exp(c_{ij})}. \quad (4)$$

By introducing a *softmax* as normalization, we force the weights to ‘compete’ with each other. As a result, PSLA can capture the most similar and critical feature in the region, similar to an attention mechanism.

We can now, in a second stage, align  $F^t$  with  $F^{t+\epsilon}$  by aggregating the corresponding feature cells with correspondence weights:

$$\hat{F}_i^{t+\epsilon} = \sum_{j \in \Phi(i)} \hat{c}_{ij} F_j^t, \quad (5)$$

where  $i$  is the index of the response of aligned feature  $\hat{F}^{t+\epsilon}$ . The procedure of aligning feature using PSLA can be formulated as  $\hat{F}^{t+\epsilon} = PLSA(F^{t+\epsilon}, F^t)$ . PSLA is the core module embedded in RFU (sect. 3.3) and DFT (sect. 3.4).

### 3.3. Recursive Feature Updating

Nearby frames may provide strong visual cues and temporal context for the inference at current frame. However, image object detectors ignore the appearance and context information from previous frames. This inspires us to propose a technique *Recursive Feature Updating* (RFU). RFU is a procedure that aggregates and integrates semantic features of sparse key frames along time, aiming to increase detection accuracy by exploiting temporal context.

Specifically, in RFU a temporal feature  $F_t$  is maintained and updated with semantic features of sparse key frames recursively throughout the whole video. During this procedure, PSLA is exploited to enforce the spatial consistence between  $F_t$  and high-level feature of new key frame. Given a high-level feature  $F_h^k$  of new key frame  $I_k$ , the operation of PSLA can be formulated as  $\hat{F}_t^k = PSLA(F_h^k, F_t)$ .

Furthermore, in order to incorporate temporal context of videos into aligned temporal feature  $\hat{F}_t^k$ , we devise a tiny

neural network, named *Update Net*, to fuse  $\hat{F}_t^k$  with  $F_h^k$  adaptively. In detail, *Update Net* takes as inputs the concatenation of  $\hat{F}_t^k$  and  $F_h^k$ . Then it produces the adaptive weights  $\hat{W}^k$  and  $W^k$  through multiple layers of convolution, where  $\hat{W}^k$  and  $W^k \in \mathbb{R}^{h \times w \times 1}$  indicate the importance of feature cells at each spatial location of two different feature maps. The weights are normalized over two feature maps for every spatial location and satisfy  $\hat{W}_{ij}^k + W_{ij}^k = 1$ . Finally  $F_t$  is updated based on the adaptive weight:

$$F_t = \hat{W}^k \cdot \hat{F}_t^k + W^k \cdot F_h^k. \quad (6)$$

The updated  $F_t$  is used in place of  $F_h^k$  to produce detection results of key frame  $I^{k'}$  and propagated to next key frame.

### 3.4. Densely Feature Transforming

After the temporal feature  $F_t$  is updated at the last key frame, the next step is to propagate it to current non-key frame for generating detection results. We introduce Dense Feature Transforming (DFT) to generate semantic features of non-key frames.

Specifically, in DFT a lower part of network  $N_f$  (denoted as  $N_l$ ) rather than the whole  $N_f$  is run on non-key frames to extract low-level features  $F_l$ , which is then used for the feature alignment performed by PSLA. Our insight is that most of frames in a video are non-key frames thus the overall computation is reduced significantly since only few sparse key frames rely on  $N_f$  to extract features. However, these low-level features do not contain sufficient semantic information to find spatial correspondence. The aligned feature may fail to preserve the critical information. To address this, a light-weight network *Transform Net* with multiple convolution layers is employed to further encode the extracted low-level features of non-key frames, aiming to approximate the high-level semantic features. This is a crucial step because it not only enriches the semantic information of low-level features but can avoid the gradients generated by feature propagation flowing into  $N_l$  directly and hence improve the robustness when training as well. The encoded feature is fed into PSLA to align  $F_t$  at previous key frame.

After propagating  $F_t$  to non-key frames, we fuse it with the low-level features  $F_l$  because the propagated features may lose some details of object appearance that are important for recognition, due to aliasing effect caused by weighted aggregation in feature alignment. To this end, a network *Quality Net* with the same structure as *Update Net* is embedded in DFT. Finally, the outputs of *Quality Net* are fed into  $N_t$  to produce detection results of non-key frames.

### 3.5. Implementation Details

We use ResNet-101 pretrained on ImageNet as  $N_f$  for feature extraction, whose layers lower than *res4b3* (including *res4b3*) are selected to construct  $N_l$ . Following [38], R-FCN is used as the task-specific network  $N_t$  for object

Methods	mAP (%)	runtime (fps)	model size (params)	Backbone
TCN [21]	47.5	-	-	GoogLeNet
TPN+LSTM [18]	68.4	2.1(X)	-	GoogLeNet
R-FCN [7]	73.9	4.05(K)	52.88M	ResNet101
TCNN [19]	73.8	-	-	GoogLeNet
DFF [38]	73.1	20.25(K)	89.95M	ResNet101
D(&T loss) [11]	75.8	-	-	ResNet101
FGFA [37]	76.3	1.36(K)	92.01M	ResNet101
FGFA [37] + [15]	78.4	1.14(K)	92.01M	ResNet101
D&T(online) [11]	78.7	6.37(X)	-	ResNet101
D&T( $\delta = 1$ ) [11]	79.8	-	-	ResNet101
MANET [32]	78.1	5(XP)	-	ResNet101
MANET [32] + [15]	80.3	-	-	ResNet101
ST-lattice [4]	79.6	20 <sup>1</sup>	-	ResNet101
STMN [34] + [15]	80.5	1.2(X)	-	ResNet101
Towards [36]	78.6	13.0(X)	-	ResNet101+DCN
Ours	77.1	30.8(V)\18.73(X)	59.04M	ResNet101
Ours	<b>80.0</b>	<b>26.0(V)\13.34(X)</b>	<b>65.79M</b>	ResNet101+DCN
Ours + [15]	<b>81.4</b>	<b>6.31(V)\5.13(X)</b>	<b>65.79M</b>	ResNet101+DCN

Table 1. Comparison of accuracy and runtime with state-of-the-art methods on ImageNet VID. Runtime is tested on different devices, where X means TITAN X, XP means TITAN XP, K means K40, Ti means 1080 Ti and V means TITAN V.

detection. The embedding function  $f(\cdot)$  and  $g(\cdot)$  in Eq.1 are implemented with a convolution layers with kernel size  $1 \times 1$ . The whole network including RFU and DFT are trained end-to-end. For hyper-parameter of PSLA, max displacement  $d$  are set as 4 by default.

*Update Net* takes two features as input, produces the fusion weights of each feature and then aggregates them based on the corresponding weights. We implement it by first reducing the features to 256 channels with  $1 \times 1$  convolution, which is followed by two  $3 \times 3$  convolution layers with 16 filters and 1 filter respectively, to produce the corresponding spatial weights for each feature. The structures of *Quality Net* and *Transform Net* are the same as *Update Net*.

*Transform Net* aims to enrich the semantic information of the low-level feature  $F_l$ . A convolution layer with  $1 \times 1$  kernel is used to reduce the feature channel to 256 and two successive convolution layers with  $3 \times 3$  kernels are appended to further encode the feature, where the last convolution layer increase the feature channel back to 1024.

## 4. Experiments

### 4.1. Dataset and Setup

We evaluate our framework on ImageNet VID [30] dataset that contains objects of 30 classes with fully annotated bounding boxes. Following the protocols in [38], we train our model on the intersection of training split of VID and subset of ImageNet DET [30] with the same categories as VID. The trained model is tested on the validation split of VID.

During training, we train the network with a batch of three images on each GPU. Each batch is sampled from either ImageNet VID or ImageNet DET at 1 : 1 ratio. When sampling from VID, We first sample an image as non-key

<sup>1</sup>The test device in this paper is not specified.

Methods	Feature Propagation	Transform Net	RFU	Quality Net
Nonlocal_S	Nonlocal [33]	✓	✗	✗
Nonlocal_F	Nonlocal [33]	✓	✓	✓
MatchTrans_S	MatchTrans [34]	✓	✗	✗
MatchTrans_F	MatchTrans [34]	✓	✓	✓
DensePSLA_S	Dense PSLA	✓	✗	✗
DensePSLA_F	Dense PSLA	✓	✓	✓
our method (a)	PSLA	✓	✗	✗
our method (b)	PSLA	✓	✓	✗
our method (c)	PSLA	✓	✓	✓

Table 2. The configuration of different methods for ablation study.

frame  $I_i$ . Then we sample another two images  $I_{k1}$  and  $I_{k2}$  near the non-key frame in a random offset. Specifically, if  $I_i$  is the  $n^{th}$  frame of a video then  $I_{k1}$  lies in  $[-l+n, -0.5l+n]$  and  $I_{k2}$  lies in  $[-0.5l+n, 0.5l+n]$ . Three images are the same when sampling from ImageNet DET. Only non-key frames are provided with training labels. Images are resized to a shorter side of 600 pixels in both training and testing. The network is trained on 8 GPU for 120K iterations using SGD. Learning rate is  $2.5 \times 10^{-4}$  in first 80K iterations and  $2.5 \times 10^{-5}$  in the last 40K iterations. During testing, we employ a fixed key frame schedule similar to [38], i.e., a video is split into segments containing equal number of frames and the middle frames are chosen as key frames. Key frame interval is set as 10 if not specified.

### 4.2. Results

We compare our framework with several state-of-the-art methods for video object detection w.r.t two aspects, trade-off and model size. The results are illustrated in Table 1.

**Trade-off** As shown in Table 1, our framework achieves 80.0 mAP at a runtime of 26.0\13.34 fps on TITAN V\X. After combining with Seq-NMS [15], our method can be further improved to 81.4% mAP and outperforms all the state-of-the-art methods to the best of our knowledge. By exploiting pixel-level and instance level calibration, MANet [32] aggregates features of 12 nearby frames to enhance the feature of reference frame. Similarly, 11 frames are exploited in STMN [34] to augment the representation of reference frame and Seq-NMS [15] is used to suppress the inconsistent detection in temporal domain, where the detection results ensemble the results from both image-based detector and the developed STMN detector. These methods increases the computation complexity significantly and not suitable in practical scenarios. Conversely our method only requires few key frames to propagate the feature and reduce much runtime while obtain results on par with them.

**Model size** Although ST-lattice [4] obtain better results than ours when using ResNet101 as backbone, an extra ResNet-101 based classifier is required by it to re-score the bounding boxes. This would significantly increase model parameters since two ResNet101 account for more than

Methods	max displacement	mAP (%)	runtime (fps)	parameters (M)
R-FCN [7]	-	73.9	4.05(X)	52.88
R-FCN*	-	74.5	10.3(V)	52.88
DFF [38]	-	73.1	20.25(K)	89.95
DFF*	-	73.5	49(V)	89.95
Nonlocal_S	-	72.5	40(V)	55.48
MatchTrans_S	2	71.4	41.2(V)	55.48
MatchTrans_S	3	72.0	40.8(V)	55.48
MatchTrans_S	4	72.0	40.6(V)	55.48
MatchTrans_S	5	72.3	40.2(V)	55.48
DensePSLA_S	2	72.9	41.2(V)	55.48
DensePSLA_S	3	73.7	40.8(V)	55.48
DensePSLA_S	4	73.6	40.6(V)	55.48
DensePSLA_S	5	73.0	40.2(V)	55.48
our method (a)	2	<b>73.6</b>	<b>42.7(V)</b>	55.48
our method (a)	3	<b>74.3</b>	<b>42.5(V)</b>	55.48
our method (a)	4	<b>74.4</b>	<b>42.0(V)</b>	55.48
our method (a)	5	<b>73.8</b>	<b>41.4(V)</b>	55.48

Table 3. Comparison of different modules for feature propagation. \* means our re-implementation.

Methods	max displacement	key frame interval	mAP(%)
DFF*	-	15	72.2
DFF*	-	25	69.7
DFF*	-	35	67.5
our method (a)	4	15	72.9 (+0.7)
our method (a)	4	25	70.5 (+0.8)
our method (a)	4	35	68.5 (+1.0)

Table 4. Comparison between PSLA and DFF at large key frame intervals. \* means our re-implementation.

100M parameters already. Instead, our method reduces the model parameters significantly and achieves competitive trade-off as well. Our method reduce the overall model size by nearly **27%** as comparing to flow based methods, *e.g.*, DFF[38] and FGFA[37]. We can not compare the model size with other flow based methods directly because the related models are not released. Theoretically, our model should be much smaller than theirs by excluding FlowNet, model size of which equals to nearly 71% of ResNet101.

### 4.3. Ablation Study

We conduct ablation study on ImageNet VID to validate the effectiveness of PSLA and the proposed framework. Firstly we introduce different variants generalized from PSLA and then make comparison between different modules for feature propagation in Table 3 and 4. The detailed setting of different methods is shown in Table 2. Next the improvement of each component on different methods is demonstrated in Table 5. Then comparison of speed-accuracy trade-off between different frameworks is shown in Fig. 4. Finally the detector is changed to Deformable R-FCN [8] to explore better performance, following [36].

Methods	max displacement	mAP(%)	runtime (fps)
our method(a)	4	74.4	42.0
our method(b)	4	75.8	31.2
our method(c)	4	<b>77.1</b>	30.8
Nonlocal_S	4	72.1	40.0
Nonlocal_F	4	74.1	28.3
MatchTrans_S	4	72.0	40.6
MatchTrans_F	4	73.0	30.1
DensePSLA_S	4	73.5	40.6
DensePSLA_F	4	75.7	30.1

Table 5. Improvement of each component on different methods. All results are tested on TITAN V.

**Methods of feature propagation** Although previous methods, *e.g.* DFF [38], mostly exploit optical flow to propagate feature maps, three variants generalized from PSLA can be used for feature propagation as well. The most intuitive one is Nonlocal [33], which attends to all positions of the feature map to establish the spatial correspondence. Another one is the dense version of PSLA, which excludes the sparsity of PSLA. We denote it as DensePSLA for simplicity. The final one is the MatchTrans module proposed in STMN [34]. It considers the local region without sparsity and performs simple normalization instead of softmax function. Experiments between these methods and PSLA are conducted to demonstrate the effectiveness of PSLA.

### Comparison between modules for feature propagation

Methods with different modules for feature propagation are compared. In particular, *Transform Net* enable stable training for PSLA and its variants thus it is added in all methods based on PSLA and its variants. The detailed configuration of compared models are illustrated in Table 2 and the results are presented in Table 3.

We re-implement R-FCN [7] and DFF [38] for fair comparison. The results are 74.5% mAP at 10.3 fps and 73.5% mAP at 49.0 fps, respectively. It can be noted that our method(a) maintains similar accuracy to R-FCN while running significantly faster. By attending to local region instead of all positions, our method(a) outperforms Nonlocal\_S by a large margin. Moreover, when comparing to MatchTrans\_S and DensePSLA\_S, our method(a) achieves better results at all max displacement and consumes less runtime as well, which demonstrates the effectiveness of the sparsity of PSLA.

As for DFF, our method(a) obtains better accuracy while significantly reduce the model parameters by nearly 38% (89.95M  $\rightarrow$  55.48M). Although our method(a) runs slightly slower than DFF, we believe more efficient feature backbone for non-key frames would narrow the gap, which we left for future work. Furthermore, in order to validate the advantage of PSLA on capturing spatial correspondence on

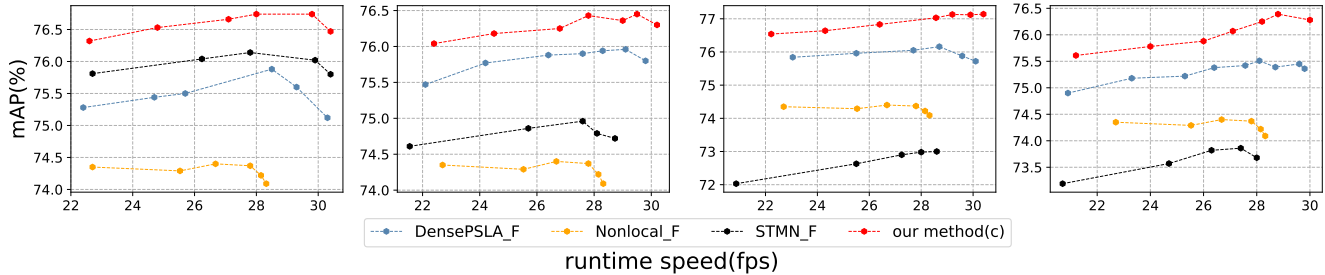


Figure 4. Speed accuracy trade-off of different frameworks. The results from left to right correspond to max displacement  $d$ , from 2 to 5.

feature maps, we compare DFF and our method(a) at larger key frame intervals where the object motion is larger. The results are illustrated in Table 4. Obviously, our method(a) performs much better than DFF. The gap between them expands when key frame interval becomes larger. It verifies that by establishing the spatial correspondence in the embedded feature map, PSLA can capture the alignment better, especially when object motion is larger.

**Improvement of each component** Now we investigate the improvement of RFU and *Quality Net* in DFT. For simplicity the max displacement is set as 4 and the models are evaluated at key frame interval of 10. As shown in Table 5, by exploiting RFU to model the temporal appearance, the performance of our method (a) is improved by 1.4%. Then *Quality Net* is incorporated to enhance the feature representation of non-key frames and it brings another 1.3% improvement. Finally the proposed framework, namely our method(c), achieves 77.1% mAP at 30.8 fps. Meanwhile, we further explore the improvement of these two components on other variants. Obviously they give a 1~2% improvement to all other variants, which demonstrate the universality of RFU and *Quality Net*.

**Comparison of speed-accuracy trade-off between different frameworks** To further demonstrate the superiority of our framework, we present the speed-accuracy trade-off of different frameworks in Fig. 4, where the max displacement is changed from 2 to 5, except Nonlocal\_F. For each result different key frame intervals are evaluated to obtain the speed and accuracy. The detailed setting of different frameworks is illustrated in Table 2. Apparently, our method (c) outperforms all other frameworks at different max displacement and achieves a better speed-accuracy trade-off.

In Figure 4 there is a trend that accuracy increases with the speed at the beginning. When the key frame interval is small, corresponding to low speed, the motion of objects between key and non-key frames is about 2 ~ 3 pixels. The small motion is hard to be captured in high-level feature map of which the receptive field is  $16 \times 16$ . In this case, PSLA may aggregate the harmful information and hurt the performance. When the key-frame interval becomes larger,

which means higher speed, the motion of objects is larger and the critical information can be captured. However, it is challenging to establish the correspondence in a constrained max displacement if the movement of objects is too large.

**More powerful backbone** Following [36], we replace the detection network with Deformable R-FCN [8] to explore better performance. The result is shown in Table 1. With a more powerful backbone, our framework achieves 80.0% mAP at 26.0 fps (TITAN V)\13.34 fps (TITAN X), which is currently the state-of-the-art speed-accuracy trade-off to the best of our knowledge. After combining with SeqNMS [15], our framework is improved to 81.4% mAP and outperform the current state-of-the-art.

#### 4.4. Extension to other tasks

The proposed framework shown in Fig. 2 could be actually used for other vision tasks beyond object detection studied in this paper. This can be easily done by replacing the task network  $N_t$  with the specific networks designed for other tasks. For example, we can replace the R-FCN used in this paper with deeplab [5] for semantic segmentation in videos. To show this point, we conducted additional experiment on CityScapes [6]. This dataset contains snippets of street scenes from 50 different cities with pixel-level labels of the 20<sup>th</sup> frame for each snippet. When training, images are sampled similar to VID and the 20<sup>th</sup> frame is set as the non-key frame. We train our framework on the training set that contains 2975 snippets and evaluate the pixel-level mean intersection-over-union (mIoU) on the validation set that contains 500 snippets. More training details are given in supplementary materials.

The results are summarized in Table 6. For fair comparison, we re-implemente the frame baseline and DFF [38] with the same setting as our method. Our method achieves very close performance to the frame baseline with higher fps, verifying the effectiveness of the proposed PSLA. It also achieves the best mIoU among the state of the arts with reasonable speed. For comparison, DFF achieves faster runtime than the baseline at the cost of accuracy by a large margin. Comparing to DVS [35], a better mIoU is achieved by ours with lower fps. Although faster, DVS relies on the

Methods	mIoU(%)	runtime (fps)
DVS [35]	70.4	19.8(Ti)
DFE [38]	69.1	5.6(K)
Frame baseline	71.1	1.52(K)
DFE (*)	69.8	8.0(V)
Frame baseline (*)	72.1	5.2(V)
Ours	71.9	6.7(V)

Table 6. Comparison of different methods on Cityscape. \* means our reimplementation.

FlowNet to propagate features, thus having much more parameters and being less preferable to practical scenarios. Such a good results on video segmentation demonstrates the universality of the proposed method for video recognition.

## 5. Conclusion

In this paper we propose a novel framework for video object detection. At its core, a novel module PSLA is proposed to propagate the feature through the whole video effectively and efficiently. By maintaining a temporal feature we model the long-term appearance of the video and improve the performance of the framework. We conduct ablation study on ImageNet VID to prove the effectiveness of our framework on video object detection. The proposed framework achieves 81.4% mAP on ImageNet VID, which outperforms state-of-the-art methods. Moreover, extensive experiment is conducted on CityScapes to demonstrate the generalization ability of the framework.

## References

- [1] D. Bahdanau, K. Cho, and Y. Bengio. Neural machine translation by jointly learning to align and translate. *CoRR*, abs/1409.0473, 2014.
- [2] A. Buades, B. Coll, and J.-M. Morel. A non-local algorithm for image denoising. In *CVPR*, 2005.
- [3] H. C. Burger, C. J. Schuler, and S. Harmeling. Image denoising with multi-layer perceptrons, part 2: training trade-offs and analysis of their mechanisms. *CoRR*, abs/1211.1552, 2012.
- [4] K. Chen, J. Wang, S. Yang, X. Zhang, Y. Xiong, C. Change Loy, and D. Lin. Optimizing video object detection via a scale-time lattice. In *CVPR*, 2018.
- [5] L.-C. Chen, G. Papandreou, I. Kokkinos, K. Murphy, and A. L. Yuille. Deeplab: Semantic image segmentation with deep convolutional nets, atrous convolution, and fully connected crfs. *T-PAMI*, 40(4):834–848, 2018.
- [6] M. Cordts, M. Omran, S. Ramos, T. Rehfeld, M. Enzweiler, R. Benenson, U. Franke, S. Roth, and B. Schiele. The cityscapes dataset for semantic urban scene understanding. In *CVPR*, 2016.
- [7] J. Dai, Y. Li, K. He, and J. Sun. R-fcn: Object detection via region-based fully convolutional networks. In *NIPS*, 2016.
- [8] J. Dai, H. Qi, Y. Xiong, Y. Li, G. Zhang, H. Hu, and Y. Wei. Deformable convolutional networks. In *ICCV*, 2017.
- [9] A. Dosovitskiy, P. Fischer, E. Ilg, P. Hausser, C. Hazirbas, V. Golkov, P. Van Der Smagt, D. Cremers, and T. Brox. FlowNet: Learning optical flow with convolutional networks. In *ICCV*, 2015.
- [10] A. Efros and T. Leung. Texture synthesis by nonparametric sampling. inproceedings of the international conference on computer vision. *ICCV*, 1999.
- [11] C. Feichtenhofer, A. Pinz, and A. Zisserman. Detect to track and track to detect. In *CVPR*, 2017.
- [12] R. Girshick. Fast r-cnn. In *ICCV*, 2015.
- [13] R. Girshick, J. Donahue, T. Darrell, and J. Malik. Rich feature hierarchies for accurate object detection and semantic segmentation. In *CVPR*, 2014.
- [14] D. Glasner, S. Bagon, and M. Irani. Super-resolution from a single image. In *ICCV*, 2009.
- [15] W. Han, P. Khorrami, T. L. Paine, P. Ramachandran, M. Babaeizadeh, H. Shi, J. Li, S. Yan, and T. S. Huang. Seq-nms for video object detection. *CoRR*, abs/1602.08465, 2016.
- [16] K. He, G. Gkioxari, P. Dollár, and R. Girshick. Mask r-cnn. In *ICCV*, 2017.
- [17] K. He, X. Zhang, S. Ren, and J. Sun. Spatial pyramid pooling in deep convolutional networks for visual recognition. In *ECCV*, 2014.
- [18] K. Kang, H. Li, T. Xiao, W. Ouyang, J. Yan, X. Liu, and X. Wang. Object detection in videos with tubelet proposal networks. In *CVPR*, 2017.
- [19] K. Kang, H. Li, J. Yan, X. Zeng, B. Yang, T. Xiao, C. Zhang, Z. Wang, R. Wang, X. Wang, et al. T-cnn: Tubelets with convolutional neural networks for object detection from videos. *T-CSVT*, 28(10):2896–2907, 2017.
- [20] K. Kang, W. Ouyang, H. Li, and X. Wang. Object detection from video tubelets with convolutional neural networks. In *CVPR*, 2016.
- [21] K. Kang, W. Ouyang, H. Li, and X. Wang. Object detection from video tubelets with convolutional neural networks. In *CVPR*, 2016.
- [22] B. Lee, E. Erdenee, S. Jin, M. Y. Nam, Y. G. Jung, and P. K. Rhee. Multi-class multi-object tracking using changing point detection. In *European Conference on Computer Vision*, pages 68–83. Springer, 2016.
- [23] S. Lefkimmiatis. Non-local color image denoising with convolutional neural networks. In *CVPR*, 2017.
- [24] T.-Y. Lin, P. Dollár, R. Girshick, K. He, B. Hariharan, and S. Belongie. Feature pyramid networks for object detection. In *CVPR*, 2017.
- [25] T.-Y. Lin, P. Goyal, R. Girshick, K. He, and P. Dollár. Focal loss for dense object detection. In *Proceedings of the IEEE international conference on computer vision*, pages 2980–2988, 2017.
- [26] W. Liu, D. Anguelov, D. Erhan, C. Szegedy, S. Reed, C.-Y. Fu, and A. C. Berg. Ssd: Single shot multibox detector. In *ECCV*, 2016.
- [27] J. Redmon, S. Divvala, R. Girshick, and A. Farhadi. You only look once: Unified, real-time object detection. In *CVPR*, 2016.

- [28] J. Redmon and A. Farhadi. Yolo9000: better, faster, stronger. In *Proceedings of the IEEE conference on computer vision and pattern recognition*, pages 7263–7271, 2017.
- [29] S. Ren, K. He, R. Girshick, and J. Sun. Faster r-cnn: Towards real-time object detection with region proposal networks. In *NIPS*, 2015.
- [30] O. Russakovsky, J. Deng, H. Su, J. Krause, S. Satheesh, S. Ma, Z. Huang, A. Karpathy, A. Khosla, M. Bernstein, et al. Imagenet large scale visual recognition challenge. *IJCV*, 115(3):211–252, 2015.
- [31] A. Vaswani, N. Shazeer, N. Parmar, J. Uszkoreit, L. Jones, A. N. Gomez, Ł. Kaiser, and I. Polosukhin. Attention is all you need. In *NIPS*, 2017.
- [32] S. Wang, Y. Zhou, J. Yan, and Z. Deng. Fully motion-aware network for video object detection. In *ECCV*, 2018.
- [33] X. Wang, R. Girshick, A. Gupta, and K. He. Non-local neural networks. 2018.
- [34] F. Xiao and Y. Jae Lee. Video object detection with an aligned spatial-temporal memory. In *ECCV*, 2018.
- [35] Y.-S. Xu, T.-J. Fu, H.-K. Yang, and C.-Y. Lee. Dynamic video segmentation network. In *CVPR*, 2018.
- [36] X. Zhu, J. Dai, L. Yuan, and Y. Wei. Towards high performance video object detection. In *CVPR*, 2018.
- [37] X. Zhu, Y. Wang, J. Dai, L. Yuan, and Y. Wei. Flow-guided feature aggregation for video object detection. In *ICCV*, 2017.
- [38] X. Zhu, Y. Xiong, J. Dai, L. Yuan, and Y. Wei. Deep feature flow for video recognition. In *CVPR*, 2017.